energies

MDPI

Article

On-Board and Wayside Energy Storage Devices Applications in Urban Transport Systems—Case Study Analysis for Power Applications

Petru Valentin Radu *, Miroslaw Lewandowski and Adam Szelag

Electric Traction Division, Power Engineering Institute, Warsaw University of Technology, Koszykowa Street 75, 00-662 Warsaw, Poland; miroslaw.lewandowski@ien.pw.edu.pl (M.L.); adam.szelag@ien.pw.edu.pl (A.S.)
* Correspondence: petru.radu@ee.pw.edu.pl; Tel.: +48-22-234-76-16

Received: 15 March 2020; Accepted: 16 April 2020; Published: 17 April 2020

Abstract: This paper investigates the benefits of using the on-board energy storage devices (OESD) and wayside energy storage devices (WESD) in light rail transportation (metro and tram) systems. The analysed benefits are the use of OESD and WESD as a source of supply in an emergency metro scenario to safely evacuate the passengers blocked in a metro train between stations; the use of OESD for catenary free sections, the benefits of using the WESD as an energy source for electrical car charging points and tram traction power supply; the benefits of using a central communication system between trams, cars, WESD and electrical car charging points. The authors investigated the use of: OESD with batteries for a catenary free section for different scenarios (full route or a catenary free section between two stations); the charge of OESD between stations (in parallel with tram motoring) to decrease the charging dwell time at stations and to help in achieving the operational timetable; the thermal effect of the additional load on the overhead contact system (OCS) when the tram is charging between stations; the sizing of OESD and WESD for emergency feeding in a metro system. The authors investigated the use of the WESD as a source of energy for the electrical car charging points to reduce the car pollution and carbon emissions. Presented in the paper is the enhanced multi train simulator with WESD prepared for the analyses conducted. The paper describes the DC electrical solver and WESD control method. A validation of the software has been conducted in regard to the substation voltage, WESD energy balance and WESD control.

Keywords: on-board energy storage device; wayside energy storage device; emergency supply; car charging points; catenary free; central communication system; electrical solver; OCS thermal analysis

1. Introduction

The European Union countries are committed to reducing the level of greenhouse gas emissions from transport by 60% by 2050 [1]. To achieve this the transport should be redirected from using fossil fuels to electricity. The European Union countries policies have been oriented on supporting the purchase of electrical cars (elimination of taxes or by giving lump sums for buying electricals cars) and to build the charging infrastructure to encourage people to buy electrical cars. A solution to eliminate car pollution in urban areas and to reduce the transport energy consumption is to have an efficient railway public transport system. To increase the traction power supply system efficiency the train braking energy needs to be returned to the distribution network or stored and later reused. There are different solutions to optimally reuse the trains regenerative braking energy like:

- Train timetable optimization—this method involves reusing the braking energy by using a train that will accelerate in the same time when the other train is braking. The optimization problem is focused on determining the optimum departure time and dwell time by using genetic algorithms

(GA) [2–6], fuzzy logic control [7], multi criteria mixed integer programing [8–10]. Studies showed that by using train timetable optimization energy savings between 15% and 35% can be achieved [2–12].

- Optimization of train speed profile and driving style—the optimization problem focuses on finding the optimal driving style and speed profile to reduce the traction mechanical energy. The authors in [13] used the direct climbing optimization which involved the calculation of optimal train speed profiles and timetable dwell time to reduce the energy consumption. The authors obtained a 14% reduction of traction energy consumption. The use of optimal train speed profile and driving style showed a reduction of energy consumption of approx. 8.4% in [14] and 8.64% in [15].
- The use of reversible substations—the conventional direct current (DC) substations are equipped with transformer rectifiers to supply the traction system. With the development of semiconductors, the use of substations with inverters is more common currently. The reversible substation provides a path for the regenerating current to flow back to the alternating current (AC) network. The recovered energy can be used in feeding the transport auxiliary consumers at stations like ventilation, lighting systems, escalators [16] or can be sent back to the main grid [16–19]. The optimization of the reversible substation is focused on minimizing the energy drawn by substation and finding the optimal size and location to achieve a good payback period. An optimization method with genetic algorithms have been used successfully in [17,18]. In [20] it is stated that by using a reversible substation (equipped with inverter in parallel with the existing transformer rectifier unit) a 13% annual reduction in energy consumption can be achieved.
- The use of on-board energy storage devices (OESD)—The OESD is located on the roof of the train, the efficiency depends on the vehicle characteristics and the type of storage technology used (batteries, supercapacitors, flywheels, hydrogen). OESD are widely used in the light transport in the past years where is required a catenary-free operation like Sapporo (Japan), Nice, Paris (France) [20], Lisbon (Portugal) [21]. The use of OESD provides the train with the possibility to run without external supply which can eliminate the overhead infrastructure from the City Centre or historical areas. Different studies focus on sizing the OESD depending on the benefits required like voltage stabilization, peak power reduction, catenary free, energy saving and CO_2 reduction [22–24]. In [23] the authors showed that if we take into account the reduction of CO_2 emissions the cost effectiveness of the OESD improves significantly which can lead to a reduced period for return of the investment. In [24] the authors demonstrated that an OESD with supercapacitors (SC) can achieve energy savings up to 18.23%.
- The use of wayside energy storage devices (WESD)—The WESD can be located in the substation, connected directly to the DC busbar or lineside of the tracks, connected to the overhead contact system (OCS). The main role of the WESD is to store the braking energy for a later use. As with the OESS the WESD can be equipped with a wide range of storage technologies (batteries, supercapacitors, flywheels, hydrogen) with the advantage that there are fewer space constraints to locate the WESD. There are different WESD manufacturers including Siemens (Sitras Static Energy Storage) implemented in Germany (Dresden, Cologne, Koln and Bochum), China (Beijing) and Spain (Madrid); Bombardier (EnerGstor) installed in Kingston (ON, Canada); ABB (Enviline) installed in Warsaw (Poland) and Hong Kong [25–30]. In [29] Ghaviha, Campillo, Bohlin and Dahlquist reviewed the use of WESD in light transport and concluded that some WESD can achieve 30% energy savings. The authors Radu and Drazek in [30] investigated the use of WESD with different types of storage technologies (lead-acid batteries, nickel metal hydride batteries, lithium ion batteries, supercapacitors and flywheels) in the Polish heavy rail transport (3.3 kV DC). The conclusion was that the WESD does not save enough energy to achieve a return on investment. According to [30] the most suitable storage technology for WESD in heavy rail transport in terms of cost is supercapacitors, however application of new types of ESD like vanadium redox flow batteries could also be taken into account [31].

The benefit of using train timetable optimization along with optimization of train speed profile and driving style is that a significant reduction in energy consumption can be achieved with minimum investment costs in modelling studies. The limitation is that these methods can't be applied in all the electrical transportation systems where the trains can't maintain a fixed dwell time like light rail transport (metro or tram systems) due to traffic conditions or other external factors. The primary scope of the light rail transport is to achieve a high frequency of trains per hour which will make it very difficult to coordinate with other trains to brake and motor at the same time. If the maximum train acceleration and speed is reduced it will provide a lower number of trains per hour and could lead to overcrowding, in the public transport, which the transport operators try to avoid.

Reversible substations can be beneficial to the traction power supply system by improving the system receptivity to train braking energy and providing the opportunity to sell the energy back to the distribution network operators or to use it to feed the station consumers. The design of the reversible substations should take into account the space constraints, location and optimal size.

The advantages of using OESD include: the option to run catenary free, the reduction in line voltage drop and increasing the train efficiency. The use of OESD can be costly if the system is designed without a traction power analysis which will provide the optimal OESS size. The increase of the train mass by using OESS will have an effect on energy consumption. Trains equipped with OESD will be more costly to maintain and may have an effect on the operation lifetime of the train.

The use of WESD can provide a set of advantages like saving braking energy for later use, mitigation of the voltage sag and reduction of the substations contracted power. Using a reversible substation with a WESD requires a traction power study to determine the optimal location and size of the equipment to achieve a good payback period.

The existing rail literature does not deal with the use of OESD or WESD to feed the train in an emergency condition, when the traction power supply is disconnected due to external factors like flooding, a fire in a metro tunnel or loss of the power supply from the distribution network operators. The OESD or WESD can supply the train for a short distance so that the passengers can be evacuated safely at the nearest station (which the authors investigated in this paper).

One of the advantages of using WESD which was not yet considered in the rail literature is to use it as charging point for the electrical cars. The working principle is to store the trains braking energy in WESD and use it later to feed the electrical cars parked at the train stations. This will also provide with the opportunity for the public to charge their electrical cars from grid at night when the electricity is cheap and sell it to the transport operator by charging the WESD. This will take the burden from the electrical distribution network. In Europe by 2040 it is planned by the European Council that the new manufactured cars to only be electrical cars. The distribution network will not be capable of supporting the increased load from the car charging points. The authors investigated this opportunity of using WESD as charging points in the paper.

The scope of this paper is to investigate the additional benefits (in addition to the well-known benefits as energy savings, peak shaving and line voltage support) of using the onboard energy storage devices and wayside energy storage devices in the light transport (metro and tram).

The paper is structured as follows: in Section 2, the electrical solver equations are presented, and the input data are discussed together with the model constraints and assumptions. The train mechanical equations and software implementation was presented by authors in [23]. Section 3 describes how the electrical solver equations and the WESD control strategy was implemented in the programming language C++. In Section 4, the authors conducted a model validation, including the substations voltage, WESD energy balance and WESD control. In Section 5, a case study has been done to test the benefits of using the WESD and OESD in an assumed metro line and tram line. The input data used in the case study is provided in Appendix A. The case study involved a detailed analysis of:

- Metro emergency feeding comparison between WESD and OESD;
- The use of OESD for a tram catenary free section and the thermal impact of the additional load on the contact wire if the OESD is charged between stations when the trams are motoring;

- The effect of tram speed on the OESD required energy capacity for the catenary free section;
- The benefits on the tram service (timetable) if the OESD is charged from the overhead contact system between stations;
- An investigation on the benefits of using the WESD as an energy source for electrical cars charging points and tram traction power supply.
- The benefits of using a central communication system between trams, electrical cars, WESD and car charging points.
- The paper findings and conclusions are presented in Section 6.

2. Mathematical Model

2.1. Model Input/Output Data and Limitations

The electrified transportation system model can be divided in two parts: in the first part the train mechanical calculations are conducted as described in [23] and the second part consists of the electrical network solver which is described in the section below.

In addition to the model inputs presented in [23], the Modeltrack (P.V.R, Warsaw University of Technology, Warsaw, Poland) software has been upgraded to include the inputs below:

- Train auxiliary power demand;
- Substation locations, rating, nominal voltage and no-load voltage;
- Substation positive feeders and return cables resistance;
- Resistance per km and length of the overhead contact system;
- Resistance per km and length of the rails;
- WESD parameters as: nominal voltage, minimum discharge voltage, state of charge (SOC), depth of discharge, efficiency (supercapacitor modules, DC-DC converter), energy capacity, power, location;
- Number of tracks;
- A complex timetable which allows entry of train dwell time at each station, headway, direction of travel and track.
- In addition to the outputs described in [23] the software output data that are obtained from the simulation model cover:
- Substations power, voltage, peak current, 60 s root mean square (RMS) current and 900 s RMS current;
- Train pantograph voltage, current, rolling resistance and speed;
- WESD total charged and discharged energy;
- WESD voltage, current, state of charge, energy, line voltage where the WESD is connected;
- The simulation software Modeltrack has the following constraints and assumptions:
- The rail traffic control system has been included only to prevent collisions between two trains on the same line;
- Trains are modeled as concentrated mass points;
- Stray currents have been omitted;
- The mass of passengers is constant from the beginning to the end of the simulated route.
- The mechanical braking is not considered to simplify the model and decrease the simulation time. This is a conservative approach and will not have a significant effect on the output results. In practice the new train type uses mechanical braking below 5 km/h.
- The train coasting mode has not been considered;

2.2. Electric Solver Equations

The electric solver of the electrified transport model is complicated to simulate because it has dynamic loads (trains) which change in time based on the line voltage and train position. To perform the load flow calculation, it uses the node potential method (nodal analysis) and Newton-Raphson [32] iterative method (1–10) which achieve fast convergence.

The voltage in nodes is calculated as in Equation (1) (where F = 0):

$$G \times V - I = 0 \tag{1}$$

G—node conductance matrix (S), V—node voltage column vector (V), I—node current column vector (A).

From Equation (2) the Jacobian matrix is calculated:

$$J = \begin{bmatrix} \frac{\partial F_{11}}{\partial V_{11}} & \cdots & \frac{\partial F_{1m}}{\partial V_{1m}} \\ \vdots & \ddots & \vdots \\ \frac{\partial F_{n1}}{\partial V_{n1}} & \cdots & \frac{\partial F_{nm}}{\partial V_{nm}} \end{bmatrix} \tag{2}$$

The derivative of function F (for trains' current) is calculated using Equation (3):

$$\left(\frac{P_{train}}{V}\right)' = -\frac{P_{train}}{V^2} \tag{3}$$

P_{train_i}—train power calculated from the vehicle movement equations (as described in [23]) (W).

The nodal voltages are calculated with Equation (4):

$$V_{(i=1)} = V_{(i=0)} - \frac{F_{(i=0)}}{J_{(V_{i=0})}} \tag{4}$$

The first node voltage iteration equation (4) can be rewritten as in Equation (5):

$$V_{(i=1)} = V_{(i=0)} - J^{-1}_{(V_{i=0})} \times F_{(i=0)} \tag{5}$$

The second node voltage iteration equation (5) can be rewritten as in Equation (6):

$$V_{(i=2)} = V_{(i=1)} - J^{-1}_{(V_{i=0})} \times F_{(i=1)} \tag{6}$$

The number of node voltage iterations (i) is repeated until the node voltage achieves the required accuracy. The node conductance matrix is calculated as in Equation (7):

$$G = G_{line} + G_{sub} \tag{7}$$

G_{line}—line (overhead contact system and rails) conductance matrix (S), G_{sub}—substation conductance matrix (substation internal resistance, positive and negative feeders) (S).

Equation (8) calculates the train current from the node voltage and electrical power taken from mechanical calculations in a given iterative step (i):

$$I_{train_i} = \frac{P_{train_i}}{V_i} \tag{8}$$

I_{train_i}—trains column vector current (A), P_{train_i}—power column vector of trains in a node (W), V_i—node voltage column vector (V).

The node voltage for a traction system without WESD can be calculated using Equation (9) in a given iterative step (i):

$$G \times V_i + \frac{P_{train_i}}{V_i} - I_{sub} = 0 \quad (9)$$

I_{sub} —substations current column vector (A):

The node voltage for WESD discharging can be calculated using Equation (10) in a given iterative step (i):

$$G \times V_i + \frac{P_i}{V_i} - I_{WESDdischar} - I_{sub} = 0 \quad (10)$$

$I_{WESDdischar}$—WESD discharging current column vector (A).

The WESD discharging current is calculated with Equation (11):

$$I_{WESD_{dischar}} = \frac{U_{SC} \times I_{SCdischar}}{U_{WESD}} \times \eta_{WESD} \quad (11)$$

U_{SC}—supercapacitor (SC) voltage (V), $I_{SCdischar}$—SC discharging current (A), U_{WESD}—Line voltage where the WESD is connected (V), η_{WESD}—WESD efficiency (DC/DC converter and SC) (%).

The node voltage for WESD charging can be calculated using Equation (12) in a given iterative step (i):

$$G \times V_i + \frac{P_{train_i}}{V_i} + I_{WESDchar} - I_{sub} = 0 \quad (12)$$

$I_{WESDchar}$—WESD charging current column vector (A).

The WESD charging current can be calculated using Equation (13):

$$I_{WESD_{char}} = \frac{U_{SC} \times I_{SCchar}}{U_{WESD} \times \eta_{WESD}} \quad (13)$$

I_{SCchar}—SC charging current (A).

The substations current column vector can be calculated from Equation (14):

$$I_{sub} = V \times G_{sub} \quad (14)$$

3. Software Implementation

The multi train simulator with WESD (Modeltrack) was developed in the C++ language. The first part of the simulator which describes train mechanical equations and software implementation was presented by the authors in [23]. The software implementation method proposed in this work is to calculate the location of the object (substation, train, WESD) in each simulation step and assigns the object to the appropriate node. In the Modeltrack software the following nodes were considered, Figure 1:

- Substation nodes—are permanent nodes (e.g., V_{11})
- Train nodes—are mobile nodes (e.g., V_{13})
- WESD nodes—are permanent nodes (e.g., V_{1m})
- Special nodes—are used to connect two or more tracks (e.g., V_{21})

The nodal conductance matrix of a given object is built of the following elements:

- G_{max}—conductance of a very high value (used to connect more tracks);
- G_l—conductance value calculated for the object on the left side (conductance calculated based on the equivalent resistance of the overhead contact system and track);
- G_r—conductance value calculated for the object on the right side (conductance calculated based on the equivalent resistance of the overhead contact system and track);

- G_{sub}—substation conductance value (conductance calculated considering the internal resistance of the traction substation, the resistance of the feeders and return cables).

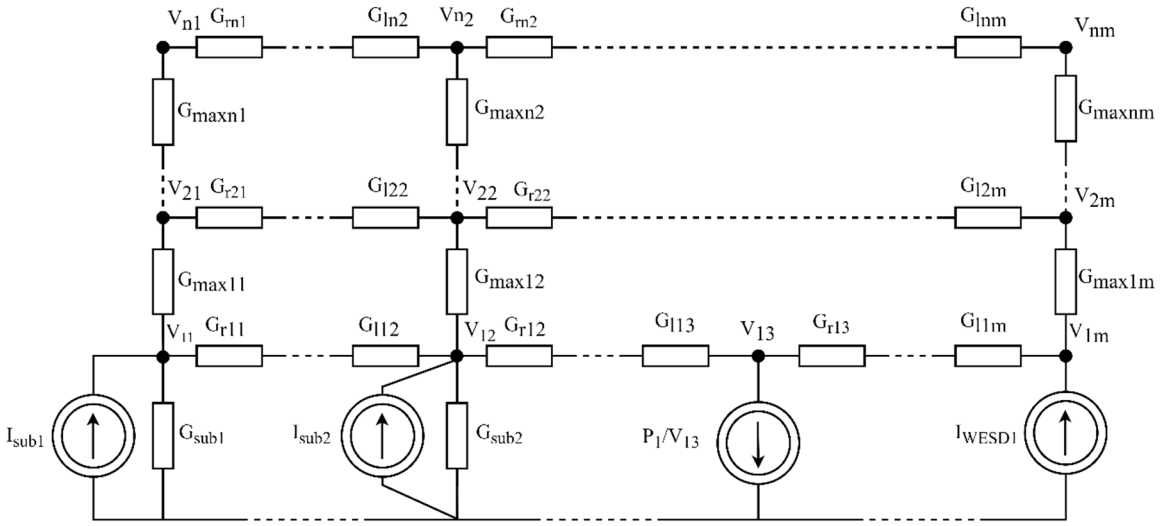

Figure 1. Multi-track section with the nodes and conductance designation.

The flowchart in Figure 2 presents the operation diagram of the electrical solver implemented in the software Modeltrack.

In the electrical solver main loop, the below main procedures are carried out sequentially:

Step 1: The program reads the output data from the train's mechanical calculations (train number, speed, power, distance) for the simulation time step (t_{step} = 1 s).

Step 2: A node is assigned automatically for each substation, train, WESD. The voltage at each node is calculated using nodal analyse and iterative process (Newton-Raphson) to determine the nodal voltage. The procedure is repeated until the calculated voltage of all nodes meets the required accuracy.

Step 3: The voltage values in nodes are stored in a temporary memory file. The voltage at the WESD node is checked against the WESD control parameters (Figure 3) and if the requirements are met (line voltage above or below the limit) the WESD will charge / discharge with a constant current.

Step 4: The voltage in each node is recalculated. If the calculated voltages do not meet the required accuracy, the program performs iterative calculations.

Step 5: The train's current is determined from the nodal voltage and calculated power. The substation's current is calculated using the node voltage and network conductance. The WESD output data are calculated (state of charge, supercapacitor voltage, energy, power, current).

Step 6: The software checks and saves the output values for the current time step and if the simulation time ($t_n \geq t_{max}$) ends, the program will terminate.

The WESD control strategy presented in Figure 3 is detailed in Table 1. The line voltage is calculated in the node where the WESD is connected.

The control strategy has two control levels which are interdependent:

- First WESD control level is named "U_{SC} control" and it determines the state of charge of the supercapacitor by measuring the supercapacitor voltage. Different control limits are used for supercapacitor charging, discharging or idle process.
- Second WESD control level is named "U_{WESD} control" and it determines how loaded the traction power supply is by measuring the line voltage in the node where WESD is connected. Different control limits are used for WESD charging, discharging or idle processes.

In Figure 3 is presented the WESD with supercapacitors control flowchart.

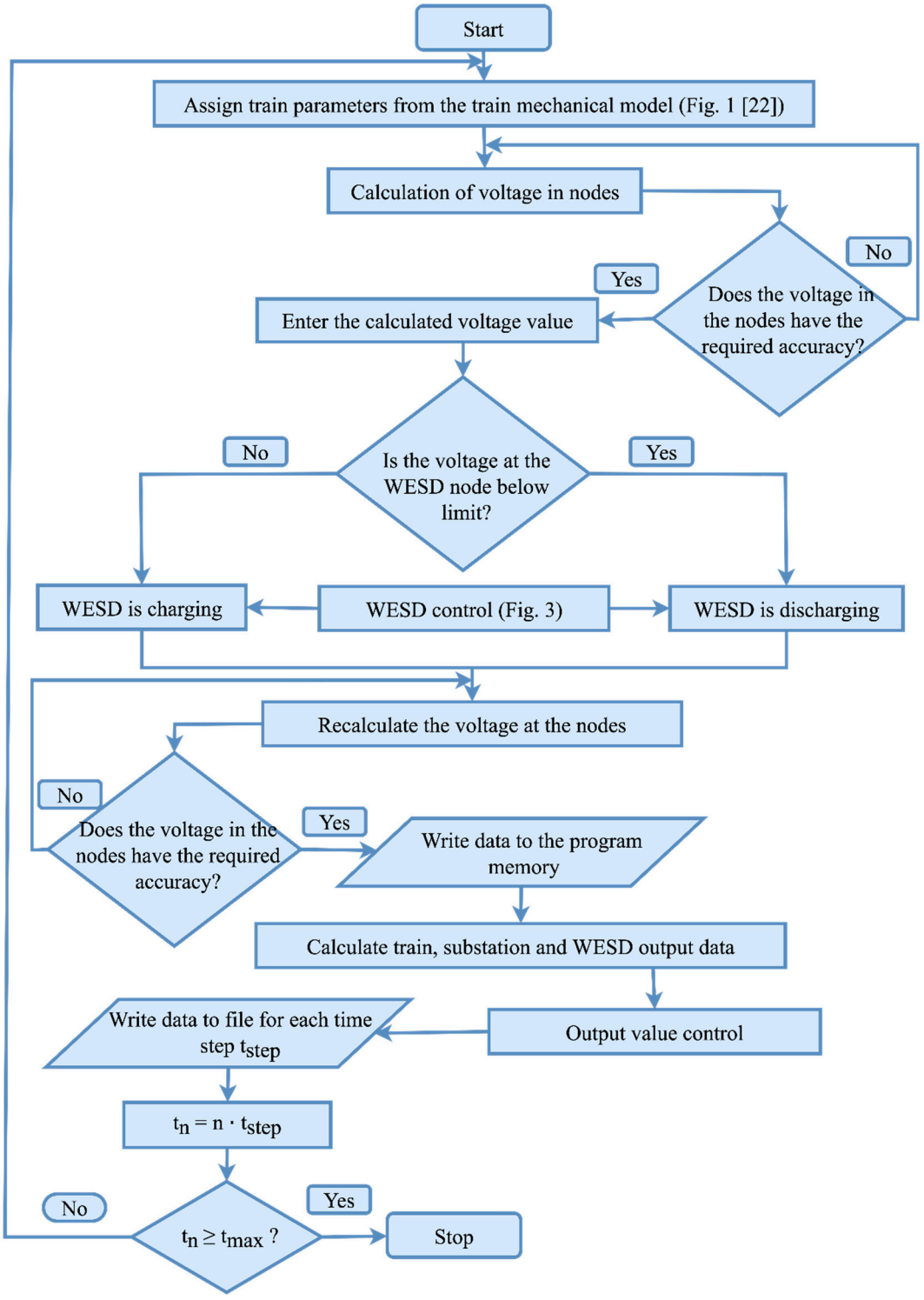

Figure 2. Flowchart of the simulation program for load flow calculations.

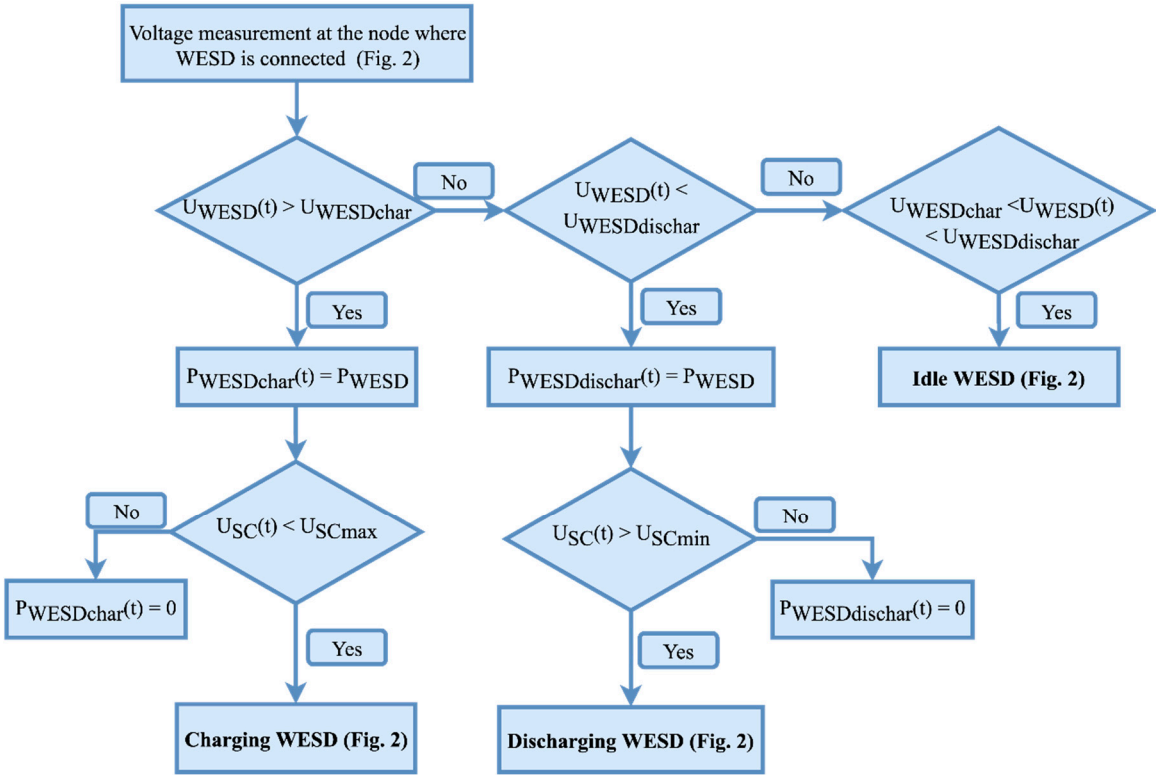

Figure 3. Flowchart of the WESD with SC control.

Table 1. WESD control strategy.

U_{WESD} Control	U_{SC} Control	WESD Control Algorithm
$U_{WESD}(t) > U_{WESDchar}$	$U_{SC}(t) < U_{SC_{max}}$	If the line voltage calculated for the time step t ($U_{WESD}(t)$) is higher than the charging control limit ($U_{WESDchar}$), the WESD will charge with the max. power ($P_{WESDchar}(t)$). The charging process will continue until the supercapacitor's cells are fully charged, the maximum supercapacitor voltage is reached ($U_{SC_{max}}$) or until the line voltage drops below the charging control limit ($U_{WESDchar}$).
	$U_{SC}(t) \geq U_{SC_{max}}$	If the WESD is fully charged it will be in the idle state until the control conditions are met for the WESD to be discharged (Idle WESD).
$U_{WESD}(t) < U_{WESDdischar}$	$U_{SC}(t) > U_{SC_{min}}$	If the line voltage is below the discharging control limit ($U_{WESDdischar}$), the WESD will discharge with max. power $\left(P_{WESD_{dischar}}(t)\right)$. The discharging process will continue until the supercapacitor cells are discharged, the minimum supercapacitor voltage is reached ($U_{SC_{min}}$) or until the line voltage rise above the discharging control limit ($U_{WESDdischar}$).
	$U_{SC}(t) \leq U_{SC_{min}}$	If the WESD is discharged it will be in the idle state until the control conditions are met for WESD charging (Idle WESD).
$U_{WESDchar} < U_{WESD}(t) < U_{WESDdischar}$	-	WESD is in the idle state for protection during quick charge or discharge process. (Idle WESD).

The described control strategy has been applied to a WESD with supercapacitors but can be used also for an WESD with batteries or any other storage technology.

4. Model Validation

To validate the electrical model, it has been assumed that a single feeder feeds each of the two lines. The tram system model input data has been presented in Appendix A. Substation 1 is located at the same location as station A. When the tram 1 starts the service from Station A (time 0 s) the line voltage should have similar values as the substation voltage (minus the losses on the feeder which are very small—feeder resistance is 0.002 Ω) as they are measured in the same location (0 km). As the tram departs the station the pantograph voltage and substation voltage will vary depending on the distance between substation and tram and the presence of other trams, Figure 4. A similar validation technique has been used in paper [33].

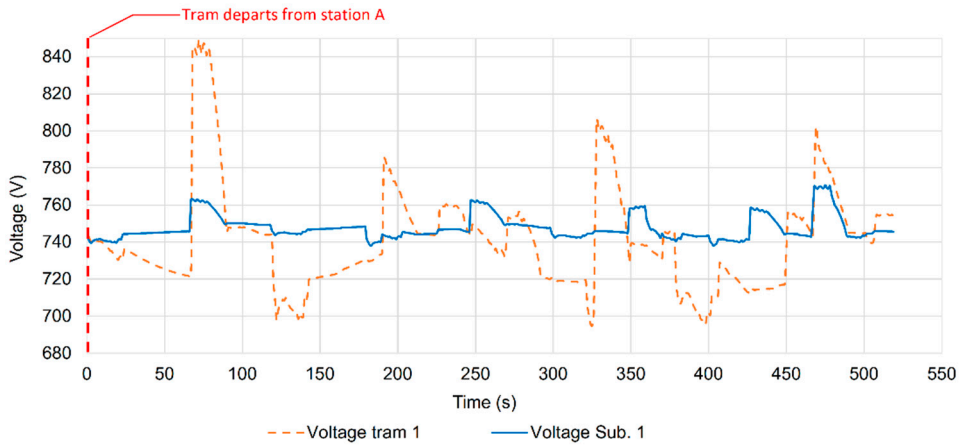

Figure 4. Simulation results (voltage tram 1 and voltage substation 1).

The tram 1 will arrive at station C at the 213 s simulation time and departs after a 30 s dwell time (243 s). Substation 2 is located at the same location (3100 m) as station C. From Figure 5 it can be observed that for the duration that the tram is parked at Station C the line voltage and the substation voltage (minus the substation losses on the feeder which are very small—feeder resistance is 0.002 Ω) have similar values.

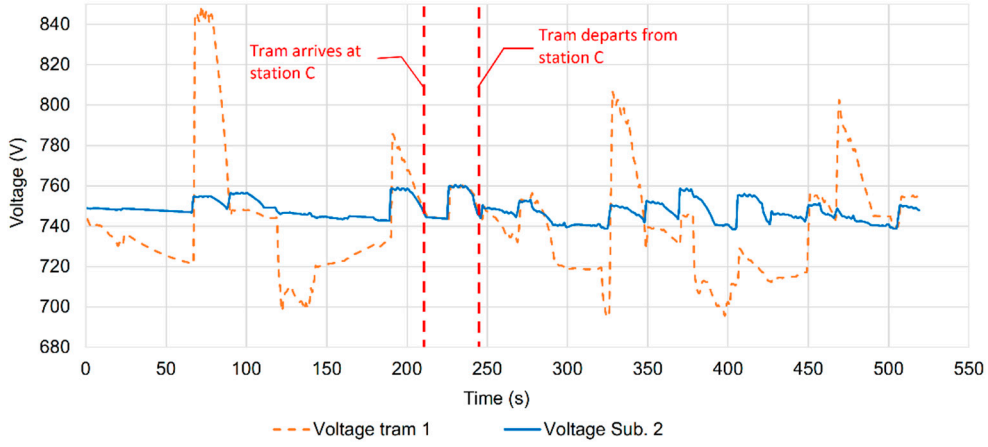

Figure 5. Simulation results (voltage tram 1 and voltage substation 2).

The tram 1 will arrive at station E at the 489 s simulation time and departs (end of route) after 30 s dwell time (519s). Substation 3 is located at the same location (7000 m) as station E. From Figure 6

it can be observed that for the duration that the tram is parked at Station E the line voltage and the substation voltage (minus the substation losses on the feeder which are very small—feeder resistance is 0.002 Ω) have similar values.

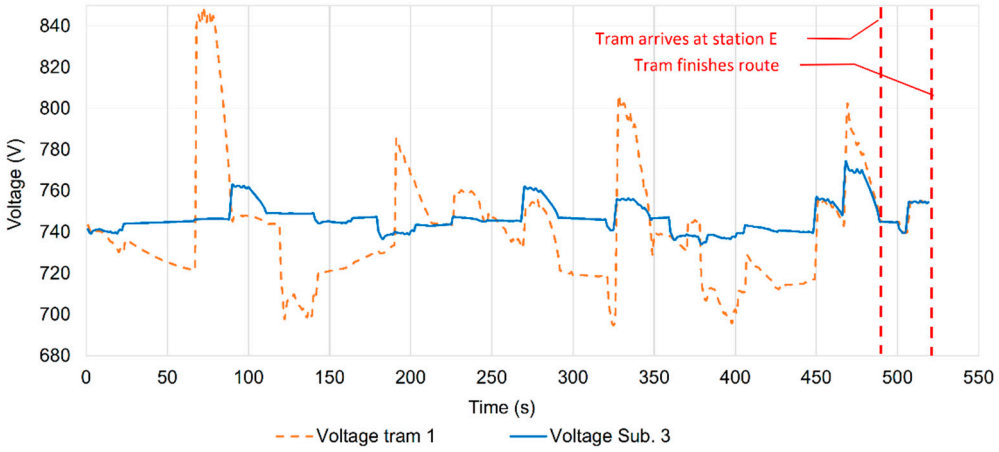

Figure 6. Simulation results (voltage tram 1 and voltage substation 3).

From the results presented in Figures 4–6 it can be concluded that the electrical model is valid. The authors conducted a validation of the WESD with supercapacitors. The WESD input parameters used in the simulation are presented in Table 2. The validation consists of checking the energy balance for charging/discharging the WESD and the WESD charging/discharging control based on the line voltage (load).

Table 2. WESD input parameters.

Parameter	Unit	Value
Location	m	5000
Capacity	kWh	5.56
Capacity	MJ	20
Nominal voltage	V	650
Efficiency (supercapacitor and DC/DC converter)	%	95
Initial state of charge	%	100
Lowest discharging voltage	V	450
State of charge for the lowest discharging voltage	%	36
Charging current	A	1500
Discharging current	A	500
Line voltage to start charge	V	760
Control idle	V	745–760
Line voltage to start discharge	V	745

For 1 h of simulation 128.2 kWh was charged into WESD and 129.6 kWh was discharged. The energy difference between charging and discharging the WESD is 1.4 kWh (129.6–128.1 kWh). The remaining energy at the end of the simulation in WESD is 4.16 kWh, Figure 7, which give a difference of 1.4 kWh (5.56–4.16 kWh). The results show that the energy balance at the beginning and the end of the simulation considering the total energy charged / discharged by the WESD is correct.

The simulation results presented in Figure 8 show that the WESD control is working according with the control requirements presented in Table 2. The WESD control results are explained below:

- WESD is charging with a maximum current of 1500 A when the node voltage, where the WESD is connected, has values above 760 V (if the state of charge allows it);
- WESD is discharging with a maximum current of −500 A when the node voltage, where the WESD is connected, has values below 745 V (if the state of charge allows it);

- WESD is idle when the line voltage where the WESD is connected is between 745 V and 760 V. The voltage buffer zone is needed to prevent against transient currents that can damage the WESD equipment.
- WESD is idle when is fully charged, state of charge 100% or discharged to the lowest state of charge value of 36%.

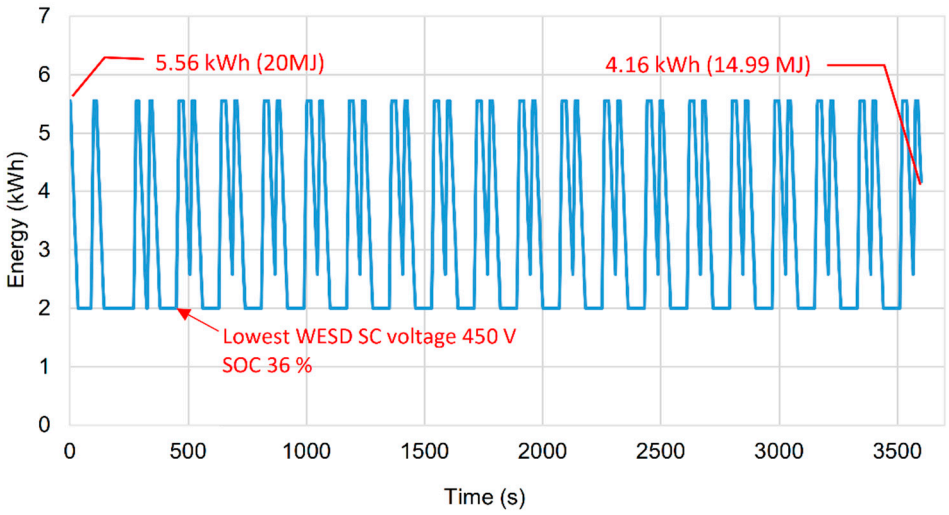

Figure 7. Simulation results (WESD energy).

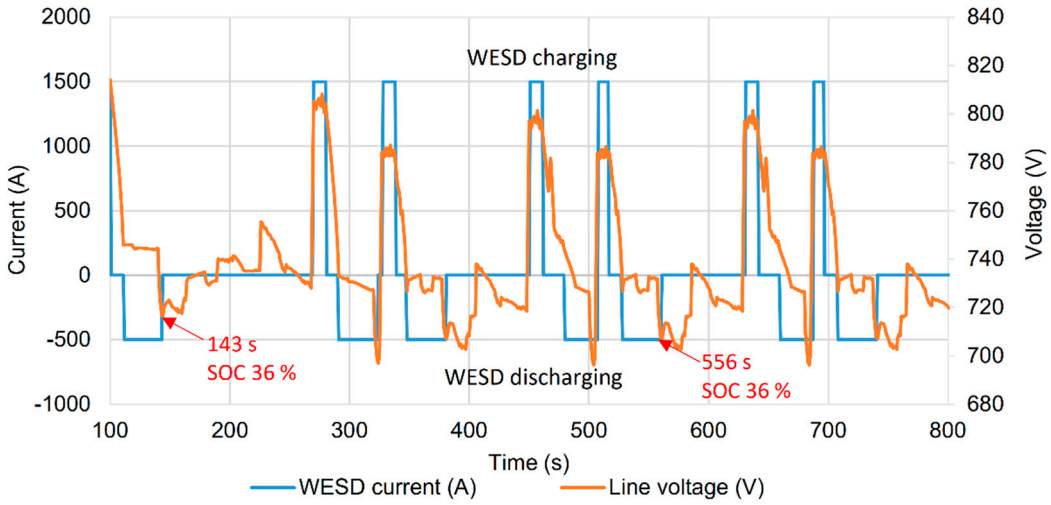

Figure 8. Simulation results (WESD current, line voltage).

When the WESD supercapacitors (SC's) are discharged (state of charge 36%) and cannot support the line load, the line voltage drops as seen in Figure 8 simulation times 143 s and 556 s.

5. Case Study

5.1. Emergency Supply in a Metro Tunnel

One of the advantages in using OESDs or WESDs is that they can supply power to the metro train in an emergency scenario. The emergency scenario can be an outage (loss of supply from the main supply point—distribution network operator) or a fire in the tunnel where the firefighters will disconnect the main supply to evacuate the passengers from the stations. From an evacuation point of

view the worst case is when the metro train is stopped in the middle between two stations. As this emergency case will require the largest amount of energy to feed the metro train.

In this section the authors calculate how much energy will be needed by the metro train to travel to the nearest station, so that the passengers can be safely evacuated. Two supplies solutions have been considered, the first solution will assume that the metro train is equipped with OESD and second solution considers an WESD that will be located at station D. The analysis was conducted for four scenarios:

- Scenario 1—the metro train is half the distance between Station A and Station B. The metro train will travel a distance of 750 m to Station B from the stationary position.
- Scenario 2—the metro train is half the distance between Station B and Station C. The metro train will travel a distance of 800 m to Station C from the stationary position.
- Scenario 3—the metro train is half the distance between Station C and Station D. The metro train will travel a distance of 950 m to Station D from the stationary position.
- Scenario 4—the metro train is half the distance between Station D and Station E. The metro train will travel a distance of 1000 m to Station E from the stationary position.

Figure 9 presents the feeding arrangement considering the WESD at station D. Substation 1, 2 and 3 will have the DC circuit breakers (CB) open. It is assumed that the metro train will travel with a safe speed of 20 km/h from the stationary position and the auxiliary load will be reduced to 1/3 (40 kWh), Appendix A, Table A6. The input data used for the simulation can be found in Appendix A.

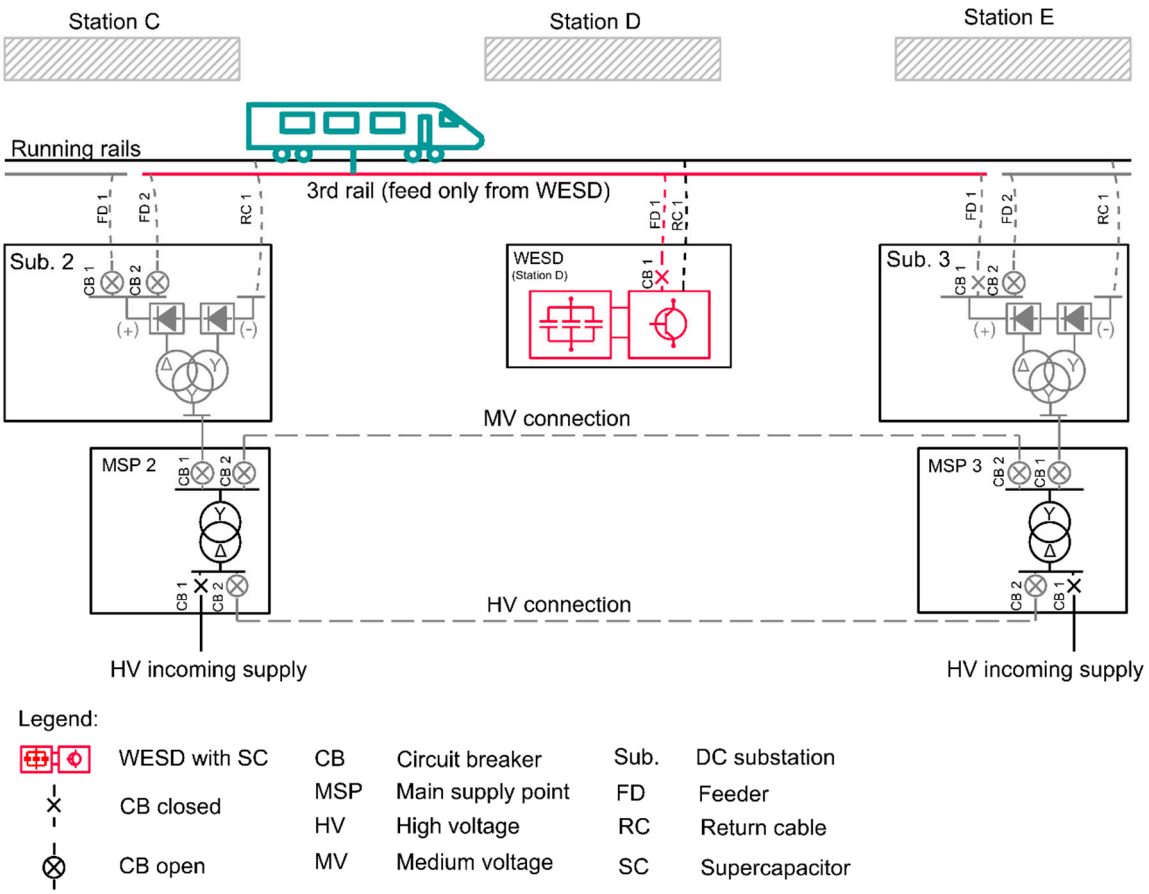

Figure 9. Emergency feeding from WESD.

The storage technology used for the WESD and OESD is supercapacitors. The supercapacitors module chosen for simulation is the BMOD0063 P125 B08SC, manufactured by the company Maxwell

Technologies (San Diego, CA, USA). The module parameters are: 125 V nominal voltage, 140 A continuous current, 1900 A maximum current, 144 Wh energy capacity and 61 kg mass [34]. To achieve 750 V line voltage, 6 SC modules should be connected in series. The minimum SC voltage for a DC/DC converter to operate should not be less than 1/3 of nominal SC voltage (minimum 250 V). In the emergency scenario it is assumed that the SC modules will fully discharge. The dimensions of a supercapacitor's module are length 619 mm, width 265 mm and height 33.3 mm. The train has four motoring carriages and the supercapacitors modules can be fixed on the roof of each carriage for the OESD scenario. It is assumed there will be an increase in mass of 13.2 tonnes (OESD energy capacity of 5.19kWh) for the metro train to account for the OESD weight [23].

Figure 10 presents the feeding arrangement considering the OESD for metro train. Substation 1, 2 and 3 will have the DC circuit breakers (CB) open. The 3rd rail will not be energized, and the metro train will be fed only by the OESD. This approach is the safest in an event of a tunnel flooding where the traction power supply needs to be disconnected.

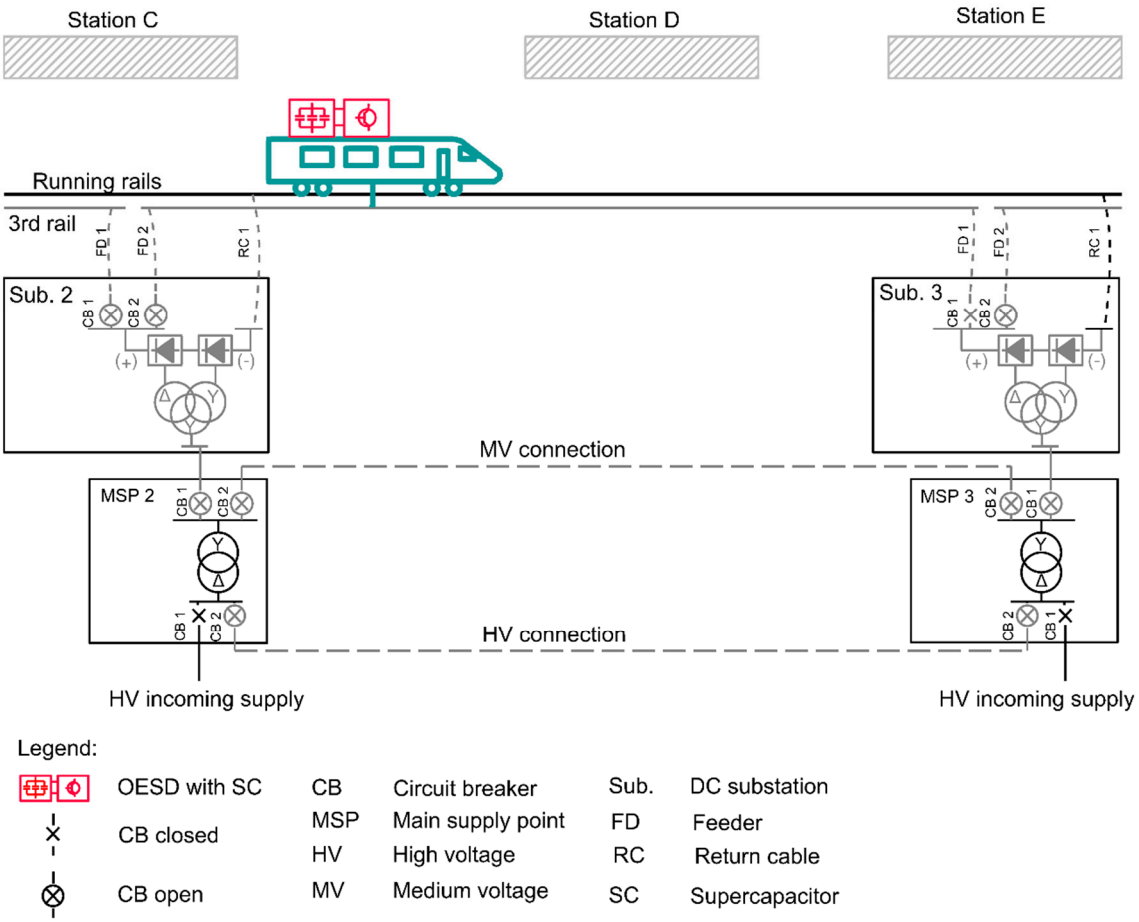

Figure 10. Emergency feeding from OESD.

If the WESD is used there will be energy transmission losses on the 3rd rail. If the metro train is equipped with an OESD it will be heavier and require more energy to feed the metro train for the same distance. The simulation results provide in Table 3 show that if the OESD is chosen the energy capacity required will be higher than in the WESD case. For the longest evacuation distance (1000 m) to station E from the middle section between station D and E, the energy capacity of the WESD should be a minimum of 6.74 kWh and the energy capacity of OESD should be a minimum of 6.88 kWh.

Table 3. WESD and OESD results for emergency feeding.

Scenario	Station	Distance between Stations (m)	Max. Evacuation Distance (m)	Duration (s)	Energy Required (kWh)	
					WESD	OESD
1	A–B	1500	750	143	5.62	5.64
2	B–C	1600	800	153	5.83	5.87
3	C–D	1900	950	180	6.33	6.74
4	D–E	2000	1000	190	6.74	6.88

5.2. Catenary Free Section

Figure 11 presents a feeding arrangement for a 750 V DC tram network with a catenary free section. The tram equipped with OESD will charge from the overhead contact system (OCS) contact wire with a reduced current, to avoid wire thermal damage and charge with a higher current at the stations where the overhead contact system is equipped with rigid overhead conductor bar [35].

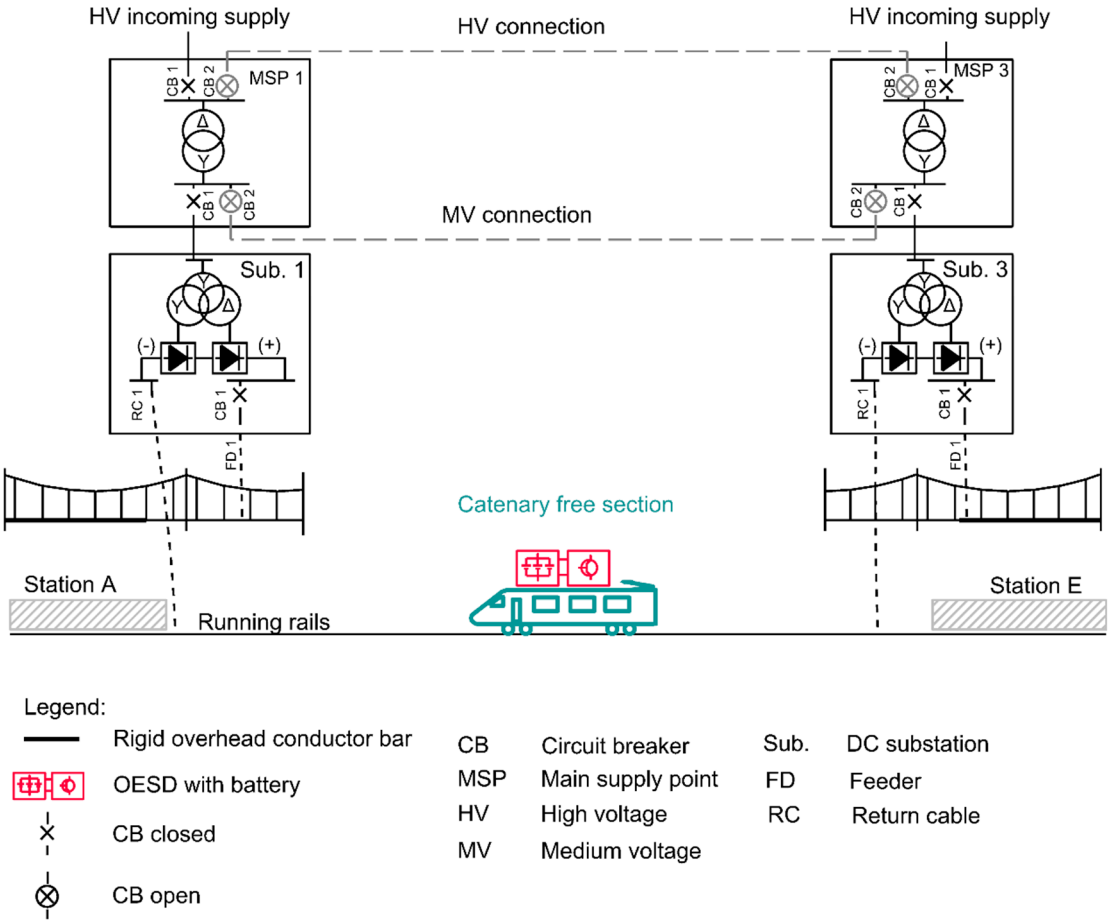

Figure 11. Catenary free section (tram fed from OESD with Li-Ion battery).

For the simulation purposes it has been considered that the tram is equipped with Li-ion battery modules type Modul Ion-12 40.30 Lithium Iron Phosphate (PFe), manufactured by the company Saft [36]. The module parameters are: 792 V nominal voltage, 90 A continuous current, 300 A maximum current (30 s discharge), 22 kWh energy capacity and 648 kg mass with liquid cooling system [36]. To achieve 450 A continuous current, 5 batteries modules should be connected in parallel. The OESD maximum energy capacity is 110 kWh for 5 batteries modules. The Li-ion cells suffers degradation over time, caused by current, temperature and other factors which influence the aging process. To mitigate the Li-ion cells degradation caused by current, temperature and other factors the batteries should not

be discharged below 400 V and charged above 750 V (to prevent overcharging) which will provide with an approximative operating energy capacity of 50 kWh (assuming energy spare for emergency situations and 6 kWh energy for cooling the OESD [36]).

The dimensions of a battery module are length 1747 mm, width 1000 mm and height 300 mm; the dimensions of the liquid cooling system module are length 1420 mm, width 430 mm and height 600 mm [36]. The tram has three motoring carriages and the modules should be fixed on the roof of each motoring carriage.

In this paper section the authors analysed six different options for different tram speeds to calculate the tram energy consumption. The OESD mass per motoring carriage has been assumed as 5 tonnes and was added to the total tram mass. Sequentially each of the line sections between stations have been assumed as catenary free sections and simulations have been run with the Modeltrack software to calculate the energy consumption. The simulation result for each option are presented in Table 4 and energy consumption per km analysis has been presented in Figure 12. Table 4 records the total energy required for a tram to run between stations A and E including the auxiliary load at stations B, C and D (30 s dwell time). The tram will charge at the first station (A) and last station (E) and the auxiliary load will not be taken from OESD at these stations.

Table 4. Simulation results for the catenary free section.

Option	Maximum Tram Speed (km/h)	Energy Required for the Catenary Free Section (kWh)				Total Energy (A–E) (kWh)
		A–B (1500 m)	B–C (1600 m)	C–D (1900 m)	D–E (2000 m)	
1	30	5.15	5.47	6.22	6.47	24.5
2	40	5.67	5.98	6.65	6.95	26.4
3	50	6.71	7.03	7.73	8	30.6
4	60	8.06	8.34	9.06	9.34	36.0
5	70	9.56	9.91	10.69	10.96	42.3
6	80	9.65	10.1	11.3	11.72	43.9

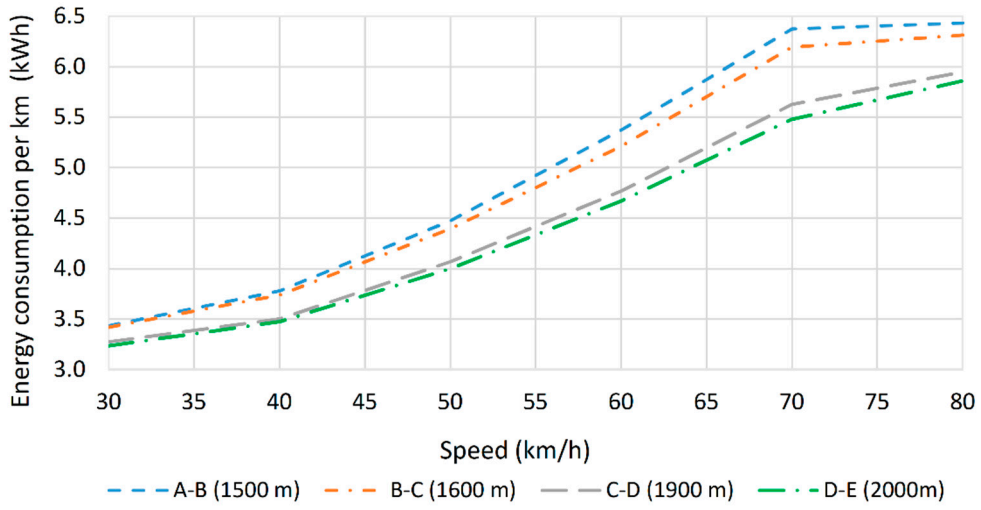

Figure 12. Tram energy consumption per km for a catenary free section.

From Figure 12 it can be observed that for a tram at lower speed the OESD will need a lower energy capacity. The average energy consumption per km is lower if a tram is travelling on a longer distance (e.g., for a speed of 80 km/h the energy consumption between A and B stations is 9% higher compared with journey between D and E stations) because at a constant speed the tram requires lower power (energy).

Equation (15) is used to calculate the OESD batteries charging time at a station until it is fully charged. The results are presented in Table 4 for a catenary free section between A and E and charging time at station A or E:

$$t_{char_{st}} = \frac{E_{OESD}}{\left(I_{OCS_{st}} \times U_{OCS} \times 0.001\right)} \times 3600 \quad (15)$$

$t_{char_{st}}$—time duration to fully charge the OESD batteries at a station (s), E_{OESD}—OESD energy capacity (kWh), $I_{OCS_{st}}$—overhead contact system charging current at station with rigid overhead conductor bar, including the auxiliary load (A), U_{OCS}—line voltage (V).

From Table 5 it can be concluded that if the line section between stations A and E is catenary free the OESD will need a significant amount of time (10 min and 25 s) to charge at a station if the line operational speed limit is 80 km/h. For a headway of 6 trams per hour an additional tram unit would be required to keep the timetable. A solution may be to make only part of the line catenary free so the OESD could charge from the overhead contact system between stations.

Table 5. Results for the catenary free section (different tram speeds).

Option	Maximum Tram Speed (km/h)	Total Energy Required to Run Catenary Free from Station A to Station E (kWh)	$I_{OCS_{st\_A}}$, $I_{OCS_{st\_E}}$ (A)	$t_{char_{st\_A}}$, $t_{char_{st\_E}}$ (s)
1	30	24.5	400	348
2	40	26.4	400	376
3	50	30.6	400	436
4	60	36.0	400	512
5	70	42.3	400	602
6	80	43.9	400	625

To investigate this, it was assumed that the line section between stations C and D is catenary free. From Table 3 can be observed that for a tram travelling with a speed of 80 km/h will need 11.3 kWh to run without an external supply between station C and D. The tram will charge from the overhead contact system ($I_{OCS_{line}}$) with a reduced current and when the tram is parked at the station A and B will charge with a fixed current ($I_{OCS_{st}}$). The maximum OESD charging from overhead contact system at stations including auxiliary load is assumed to be 400 A. The maximum energy that can be charged into OESD at each station for a 30 s dwell time was calculated as 2.11 kWh. The OESD will need to be fully charged before leaving station C which may affect the fixed dwell time of 30 s:

$$E_{OESD} = E_{OCS_{st\_A}} + E_{OCS_{st\_A-B}} + E_{OCS_{st\_B}} + E_{OCS_{st\_B-C}} + \cdots + E_{OCS_{st\_n}} + \cdots + E_{OCS_{st\_n-(n-1)}} \quad (16)$$

$E_{OCS_{st\_A}}$—energy charged into OESD from overhead contact system at station A, $E_{OCS_{st\_A-B}}$—energy charged into OESD from overhead contact system between station A and station B, $E_{OCS_{st\_B}}$—energy charged into OESD from overhead contact system at station B, $E_{OCS_{st\_B-C}}$—energy charged into OESD from overhead contact system between station B and station C.

In Table 6 different values were considered for the OCS charging current between stations to see how the charging time can be reduced at station C.

Table 6. Results for the catenary free section between stations C and D.

$I_{OCS_{line}}$ (A)	$E_{OCS_{st\_A-B}}$ (kWh)	$E_{OCS_{st\_B-C}}$ (kWh)	$E_{OCS_{st\_C}}$ (kWh)	$t_{char_{st\_C}}$ (s)	Service Affected
50	0.94	2.23	3.9	56	Yes
60	1.13	2.68	3.3	47	Yes
70	1.31	3.12	2.7	38	Yes
80	1.50	3.57	2.0	29	No
90	1.69	4.01	1.4	20	No
100	1.88	4.46	0.8	11	No

If the OESD is charged from the overhead contact system between stations with a minimum current of 80 A the station 30 s dwell time and the tram service will not be affected. For a 50 A charging current the tram service is delayed by 26 s (Table 6).

The increase in load for the overhead contact system will increase the wire temperature which can affect the mechanical properties of the material. To assess the increase of the overhead contact system contact wire temperature with load the authors conducted an analysis for the OCS system without OESD and with OESD for a line charging current of 100 A. The methodology to calculate the wire thermal resistance and temperature has been calculated similar to [37–39]. The input data for the contact wire temperature calculation is presented in Table A5, Appendix A7. The Modeltrack software was used to calculate the maximum overhead contact system current between the Station B and Station C for an operational service of 20 trams per hour per direction (3 min headway). The load between the catenary wire and contact wire was calculated based on wire resistance.

Figure 13 presents the contact wire temperature calculation results for a train with OESD charging from the overhead contact system between stations and a train without OESD charging from overhead contact system between stations.

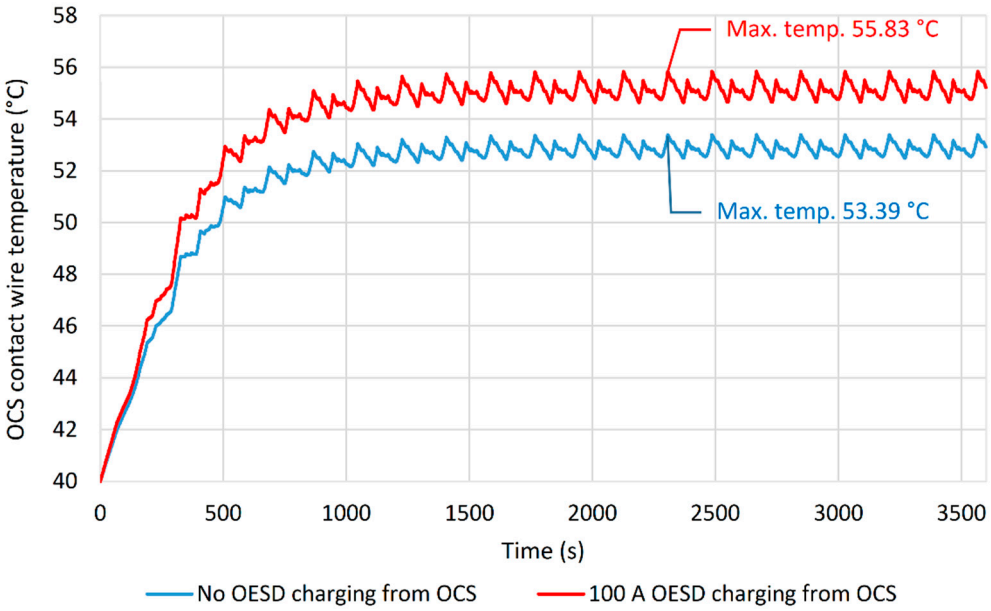

Figure 13. Maximum contact wire temperature between Station B and Station C.

From Figure 13 can be observed that if the OESD is not charged from overhead contact system between station the maximum overhead contact system contact wire temperature is 53.39 °C. For a 100 A maximum OESD charging current between stations the overhead contact system contact wire temperature rises to 55.83 °C.

5.3. WESD for Electrical Cars Charging Points Investigation

The integration of the electrical car charging point (ECCP) into the local grid is one of the biggest challenges in future for the distribution network operators. Most of the existing power grids in Europe were not designed for the power demand/load fluctuations that charging points requires. If the charging points are analysed as a single load it doesn't make a big impact on the grid but if we consider the peak time when multiple charging points are used, the impact on the grid stability can be significant [40,41]. The charging points can be classified in 3 main groups depending on power, voltage, number of phases (single phase or 3-phase), type of charging current (AC or DC) [40–43]:

- I ECCP group—230 V AC (single phase), charging power up to 3.7 kW for domestic use. The charging time for this group can range between a few hours up to 10 h for full charge.

- II ECCP group—230 / 400 V AC (single phase or 3-phase) or DC, charging power up to 22 kW (Nissan Wallbox 7 kW, Tesla Wall Connector 22 kW) for domestic use or installed in residential areas or public car parks. The charging time for this group can range between half hour up to 2 h for full charge.
- III ECCP group—600 V / DC, charging power 120 kW (Tesla Supercharger), 200 kW–350 kW installed in location as car rental companies, fleet of company cars or service stations. The fast charge ECCP can charge the battery of a car in a few minutes.

In Figure 14 a supply arrangement for the charging point from WESD is proposed. The tram braking energy is to be stored in WESD which in turn will be feeding the charging point. The charging points are to be installed in car parks in the close vicinity of tram stations to encourage people to use the public transport.

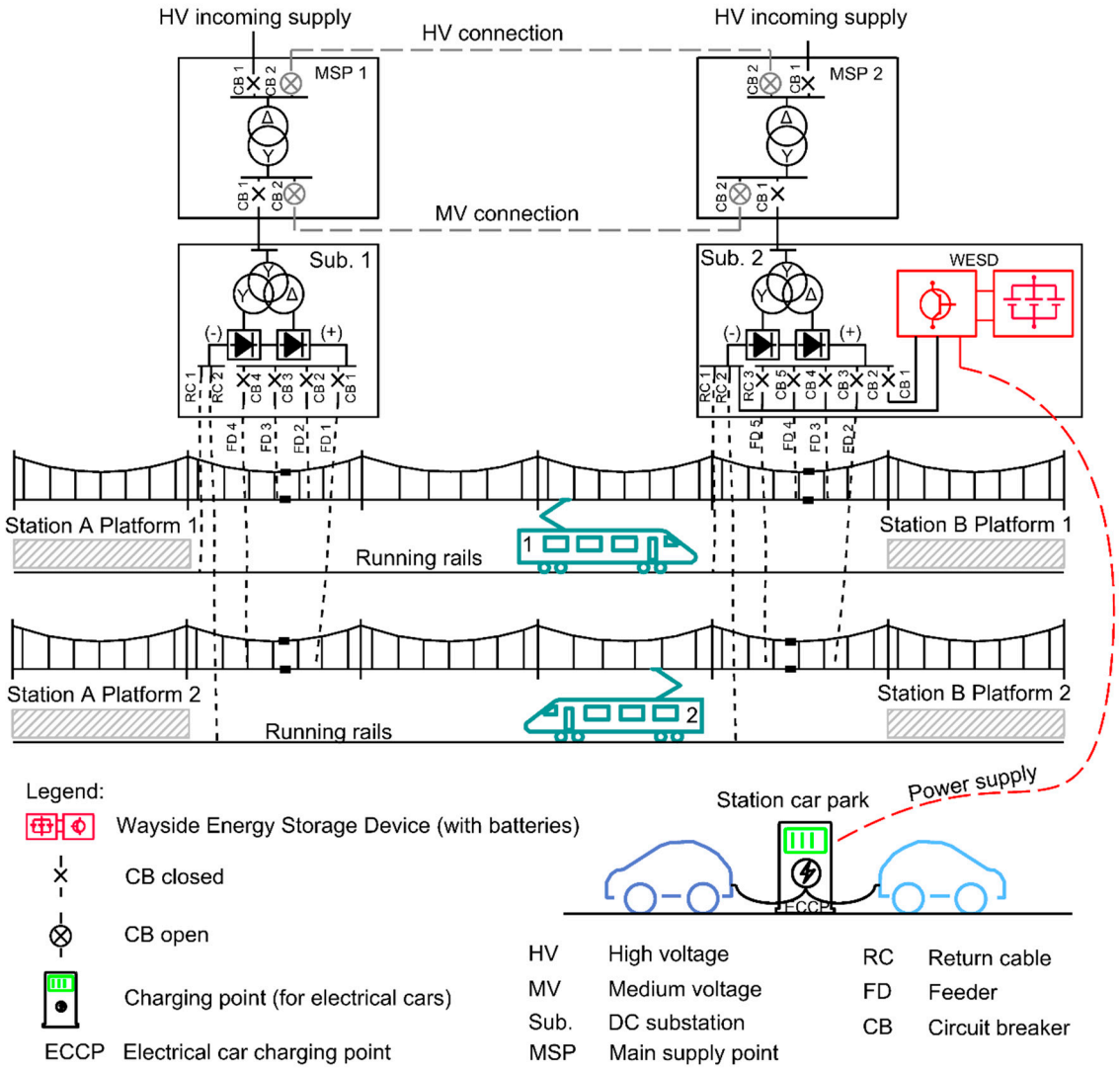

Figure 14. Feeding arrangement with charging point and WESD.

As the tram load is fluctuating and the tram traction connected power is higher than the tram's requirements at a given time there is power spare capacity for certain period of times. The traction load can be monitored, and an energy management system can control the charge of the WESD from the overhead contact system if the there is no significant load on the overhead contact system. If there is no requirement for the charging point to charge the cars in a specific period of time, the braking

energy can be reused from the WESD to supply the traction load. If the charging points are designed to be bidirectional, the cars can be charged at home after peak time, when the electricity is cheap and partial discharged into the charging point (WESD) the next day. This energy can be used to charge other cars or support the traction load. The tram transport operators can give a discount on public transport to the car owners who sell energy to them through charging points.

Figure 15 presents the proposed system communication architecture. The overhead contact system and traction power supply system has been omitted from the figure for better visibility.

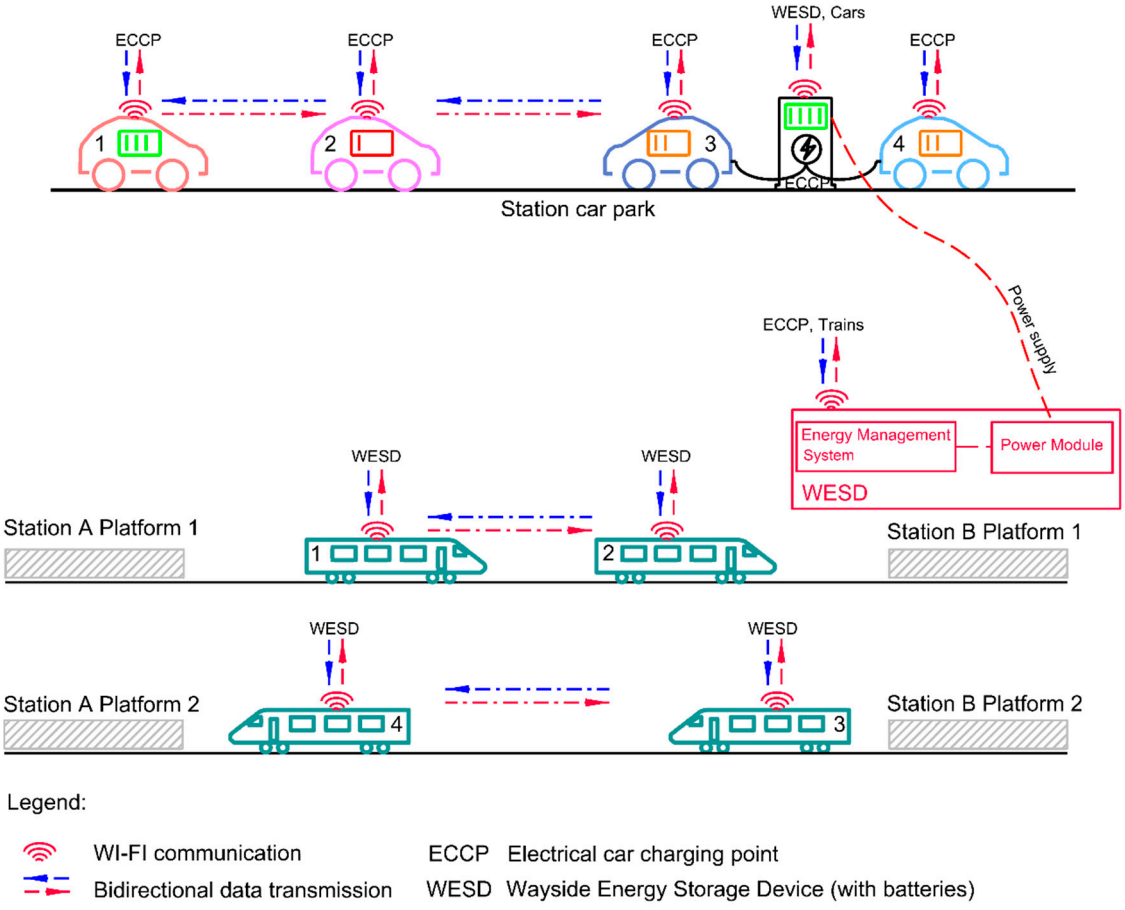

Figure 15. Communication architecture between charging point, trains, cars and WESD.

The system includes the following subsystems (Figure 16):

- The electric car system may comprise:
  - Communication Module—communicates with the charging point the car location, battery parameters (power, energy capacity, state of charge) and the required action (if the car will charge or discharge at the charging point);
  - Display Module—it allows the car user to communicate with the charging point for charging availability and car Central Control Unit to check the batteries state of charge;
  - Display Module—it allows the car user to communicate with the ECCP for charging availability and car— Central Control Unit to check the batteries SOC;
  - Central Control Unit—is the unit where all the information's are processed and controls the car battery system.
- The tram system may comprise:
  - GPS Module—locates geographical position of the tram with the GPS;

- Communication Module—communicates with the WESD the tram location and tram motion state (acceleration, braking, coasting) and speed values.
- Central Control Unit—provides the tram Communication Module with the tram motion state and speed values.

- The electric car charging point may comprise:
  - Communication Module—communicates with the cars and WESD regarding the charging availability and WESD batteries state of charge.
  - Data Storage Unit—it stores the information received from the cars and WESD.
  - Power Module—is the power interface between the charging point and cars.
  - Central Control Unit—controls the cars charging / discharging process.
- The WESD may comprise:
  - Power Module—includes the batteries modules, DC/DC converter, data acquisition unit and communication module. This module provides the electrical energy for the ECCP.
  - Energy Management System—includes the communication module, data storage unit and central control unit. The scope of this system is to take the main decision regarding the WESD charging/discharging based on trams position and charging point charging / discharging requirements.

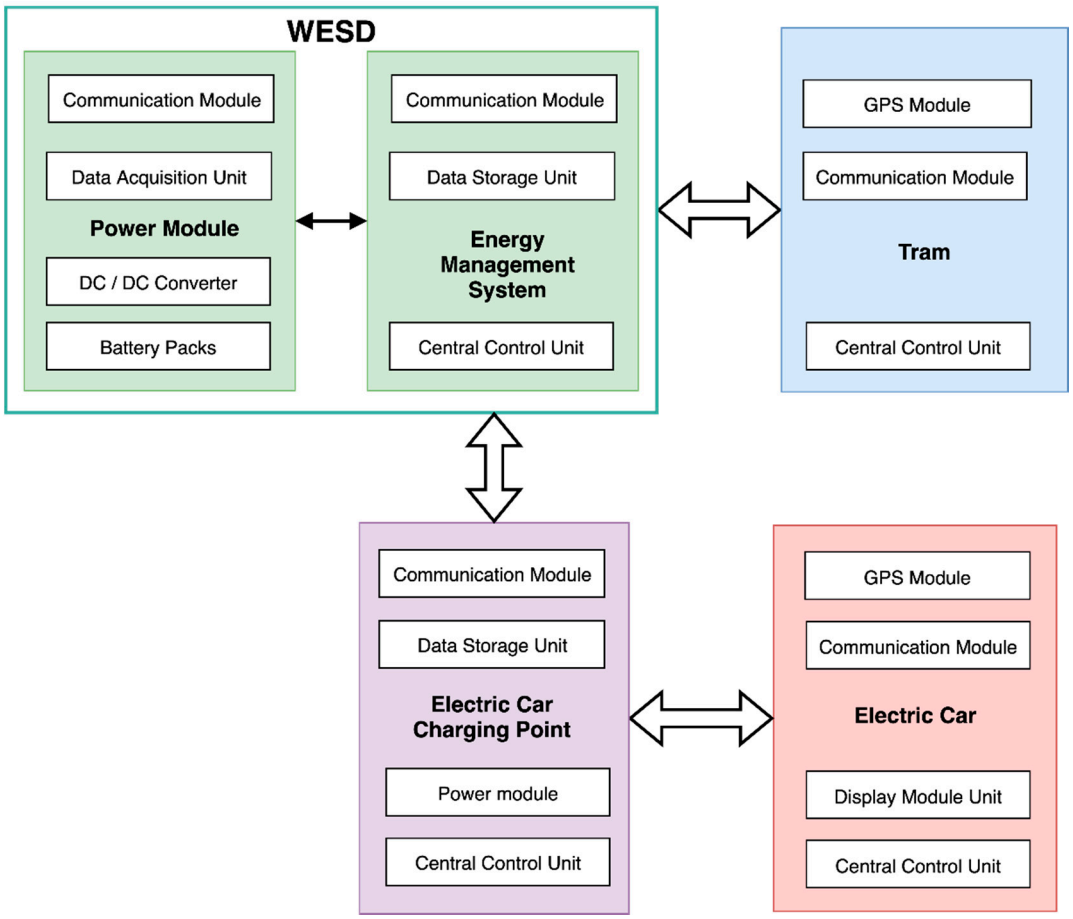

Figure 16. Control and supply system architecture for ECCP with WESD.

6. Conclusions

The Modeltrack multi train modelling software is a useful tool to model all types of DC transport systems for research or design purposes. The paper presented the electrical solver main equations, WESD control strategy and programing implementation. A mathematical validation of the software has been conducted with good results.

The OESD and WESD can be used to feed the metro train in an emergency scenario (loss of traction supply) to transport the passengers at the nearest station. It was noticed that the required energy capacity for the storage system is comparable in both cases (between 1 and 6% less energy required for WESD compared with OESD). When WESD is used there will be energy losses on the overhead contact system but when the OESD is used the losses will be due to increased mass of the metro train. Each of the options have benefits and disadvantages depending on the required system functionality. The simulation results show that the tram average energy consumption per km is lower if a tram is travelling on a longer distance (9% energy reduction for a 25% distance increase). The tram speed has a significant impact on the required OESD size for the catenary free section. A tram speed increase from 30 km/h to 80 km/h will require an additional 80% energy capacity for the OESD.

From the analyses conducted on trams for catenary free sections it can be concluded that charging the OESD from overhead contact system between stations can reduce the charging time at stations by a few minutes. The charging current between stations has a significant impact on the tram dwell time. For a 50 A charging current from the contact system between stations the tram will encounter a maximum delay of 26 s. It was found that the additional charging load from the overhead contact system can have a thermal effect on the contact wire (temperature changing from 53.39 °C to 55.83 °C). If the OESD is charged only at the first and last station the tram service timetable will be affected. This can be avoided if the overhead contact system is designed for a higher charging power at stations using rigid overhead conductor bar to avoid thermal stress on the contact wire.

The benefits of using WESD working with car charging point can be:

- No distribution network connection is required for the car charging point;
- The tram braking energy can be reused for charging the electrical cars;
- The braking receptivity of traction power supply system can be increased by using WESD;
- If the electrical car charging point (ECCP) is bidirectional the traction load can be reduced;
- The costs of purchasing electrical energy from the distribution network can be reduced if the public provides cheaper of-peak energy from their cars;
- The public will be encouraged to use the public transport supporting the decarbonization process of cities.

Author Contributions: All authors have worked on this manuscript together and all authors have read and agreed to the published version of the manuscript. Conceptualization, P.V.R., M.L. and A.S.; formal analysis, P.V.R., M.L. and A.S.; methodology, P.V.R., M.L. and A.S.; software, P.V.R.; validation, P.V.R., M.L and A.S.; data Curation, P.V.R., M.L. and A.S.; writing—original draft preparation, P.V.R., M.L. and A.S.; writing—review and editing, P.V.R., M.L. and A.S.; supervision, M.L. and A.S.

Funding: This research received no external funding.

Conflicts of Interest: The authors declare no conflict of interest.

Nomenclature

Be	Braking effort (N)
CB	Circuit breaker
CCS	Central communication system
CCU	Central communication unit
ECCP	Electrical car charging point
$E_{OCS_{st\_A}}$	Energy charged into OESD from OCS at station A (W)
$E_{OCS_{st\_A-B}}$	Energy charged into OESD from OCS between station A and station B (W)

E_{OESD}	OESD energy capacity (kWh)
ESD	Energy storage device
FD	Substation positive feeder
G	Node conductance matrix (S)
Gline	Line (OCS and rails) conductance matrix (S)
Gsub	Substation conductance matrix (substation internal resistance, positive and negative feeders) (S)
HV	High voltage (e.g., 110 kV)
i	Iterative step
I	Node current column vector (A)
$I_{OCS_{st}}$	OCS charging current at station with rigid overhead conductor bar, including the auxiliary load (A)
I_{SCchar}	SC charging current (A)
$I_{SCdischar}$	SC discharging current (A)
I_{sub}	Substation current (A)
I_{train}	Trains current column vector (A)
$I_{WESDdischar}$	WESD discharging current (A)
$I_{WESDchar}$	WESD charging current (A)
J	Jacobian matrix
Li-ion	Lithium—ion (battery)
MSP	Main supply point
MV	Medium voltage (e.g., 15 kV)
OCS	Overhead contact system
OESD	On-board energy storage device
P_{train}	Train power column vector (W)
$P_{WESDchar}$	Max. charge power, WESD control parameter (W)
$P_{WESDdischar}$	Max. discharge power, WESD control parameter (W)
RC	Return cable to substation negative busbar
RMS	Root mean square
RR	Rolling resistance (N)
SC	Supercapacitor
SOC	State of charge (%)
Sub.	DC substation
t	Simulation time step (s)
Te	Tractive effort (N)
$t_{char_{st}}$	Time duration to fully charge the OESD batteries at station (s)
t_{max}	Duration of the entire simulation (e.g., 1 h)
t_n	Time duration elapsed of the simulation (e.g., 100 s)
t_{step}	Duration of the simulation time step (e.g., 1 s)
$U_{SC_{min}}$	Minimum SC voltage, control parameter (SC discharged) (V)
$U_{SC_{max}}$	Maximum SC voltage, control parameter (SC charged) (V)
U_{OCS}	Line voltage (V)
U_{WESD}	Line voltage where the WESD is connected (V)
$U_{WESDchar}$	WESD voltage charging control parameter (V)
$U_{WESDdischar}$	WESD voltage discharging control parameter (V)
v	Tram/metro velocity (km/h)
V	Node voltage column vector (V)
WESD	Wayside energy storage device
η	Efficiency of the train motors at different velocity (%)
η_{WESD}	WESD efficiency (DC/DC converter and SC) (%)

Appendix A

Tables A1–A7 present typical input parameters used for simulation purposes in this paper. The information in the tables have been sourced from equipment manufacturers, technical papers or assumed according with engineering common practice [21–30,32–38].

Table A1. Substations input parameters.

Substation No.	Nominal Voltage (V)	No Load Voltage (V)	Rating (MW)	Location (m)	Feeder Resistance (Ω)
Substation 1	750	785	1 × 2	0	0.002
Substation 2	750	785	2 × 2	3200	0.002
Substation 3	750	785	1 × 2	7000	0.002

Table A2. Stations input parameters.

Station No.	Location (m)	Dwell Time (s)
Station A	0	30
Station B	1500	30
Station C	3100	30
Station D	5000	30
Station E	7000	30

Table A3. Tram supply system input parameters.

Parameter	Type	Material	Electrical Resistance (Ω/km)	Wear (%)
Contact wire	1 × 120 mm^2	Cu	0.153	30
Catenary wire	1 × 161 mm^2	Cu	0.110	–
Rail	60 kg/m	steel alloy	0.033	10

Table A4. Metro train supply system input parameters.

Parameter	Type	Material	Electrical Resistance (Ω/km)	Wear (%)
3rd rail	3800 A	aluminum/steel	0.00885	5
Rail	60 kg/m	steel alloy	0.033	10

Tables A5 and A6 present typical tram and metro-train parameters assumed for simulation purposes.

Table A5. Tram input parameters.

Parameter	Unit	Value
mass of tram with passengers	tonne	75
voltage	V	750
maximum tractive effort	kN	94
auxiliary load	kW	47
number of carbodies	–	5
number of motoring carriages	–	3
number of motors per motoring carriage	–	4
carriage width	m	2.8
tram length	m	35
maximum acceleration rate	m/s	1.2
mean braking service rate	m/s	1.1
rotating mass factor	–	1.07

Table A6. Metro train input parameters.

Parameter	Unit	Value
mass of metro train	tonne	160
passenger mass	tonne	100
voltage	V	750
maximum tractive effort	kN	266
auxiliary load	kW	120
number of motoring carriages	–	4
number of trailer carriages	–	2
number of motors per motoring carriage	–	4
carriage length	M	20
carriage width	M	2.8
maximum acceleration rate	m/s	1.1
mean braking service rate	m/s	1
rotating mass factor	–	1.08

Figure A1 presents the assumed tram tractive effort (Te), braking effort (Be), efficiency (η) and rolling resistance (RR) curves as a function of velocity (v). It can be noticed from Figure A1 that the tram rolling resistance increases with the velocity.

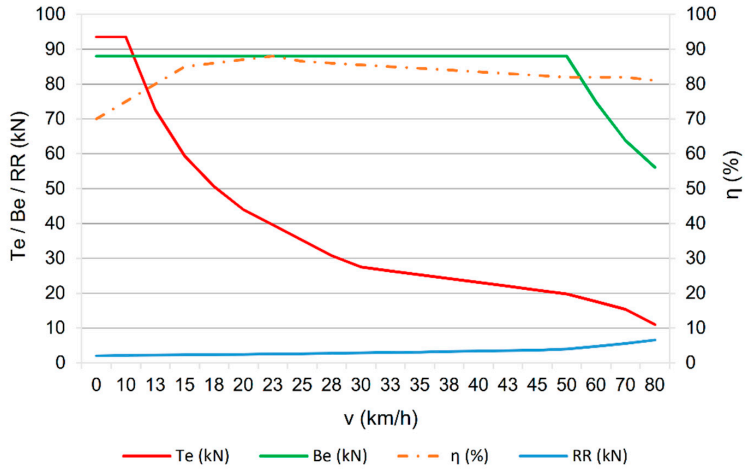

Figure A1. Tram tractive effort, braking effort, rolling resistance and efficiency as a function of velocity.

Figure A2 presents the assumed metro train tractive effort (Te), braking effort (Be), efficiency (η) and rolling resistance (RR) curves as a function of velocity (v). It can be noticed from Figure A2 that the metro train rolling resistance increases with the velocity.

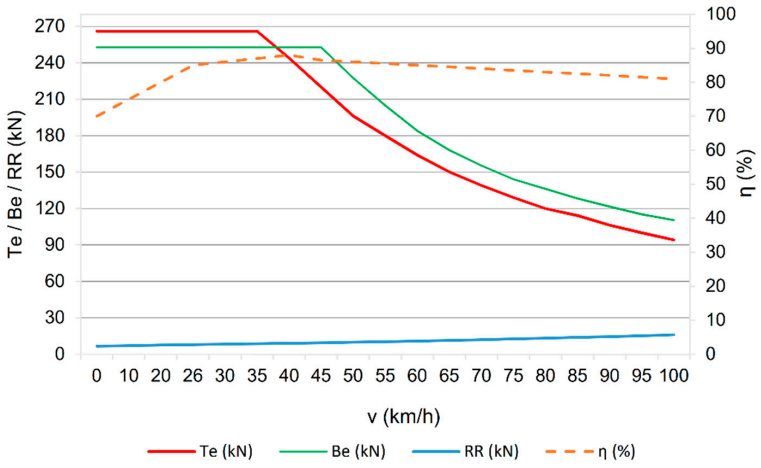

Figure A2. Metro train tractive effort, braking effort, rolling resistance and efficiency as a function of velocity.

Figures A3–A5 present 1 h of tram operation for a headway of 3, 10 and 12 min (30 s dwell time).

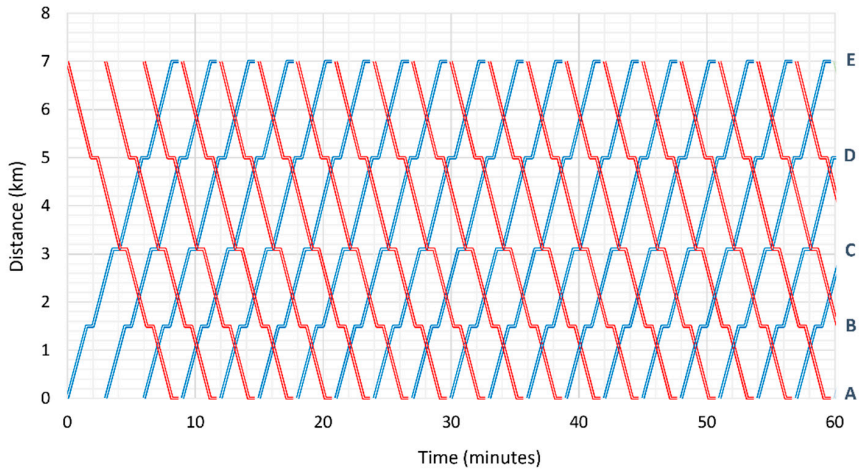

Figure A3. Simulation of 1 h tram operation between station A and B and return (3 min headway, 30 s dwell time).

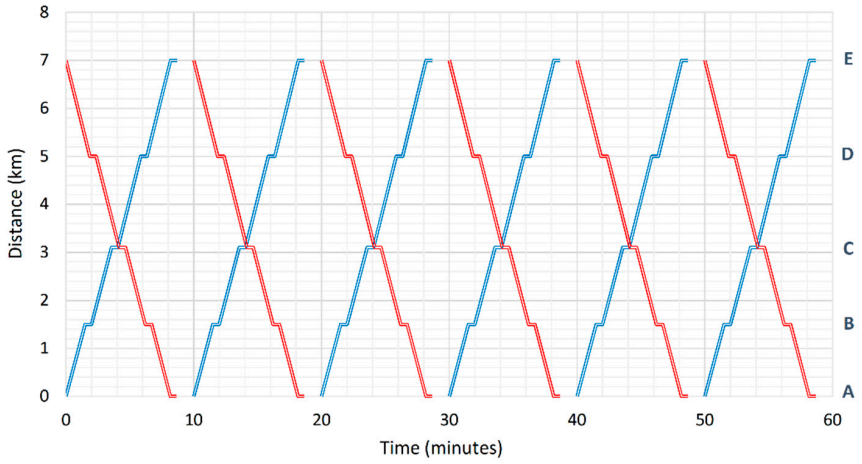

Figure A4. Simulation of 1 h tram operation between station A and B and return (10 min headway, 30 s dwell time).

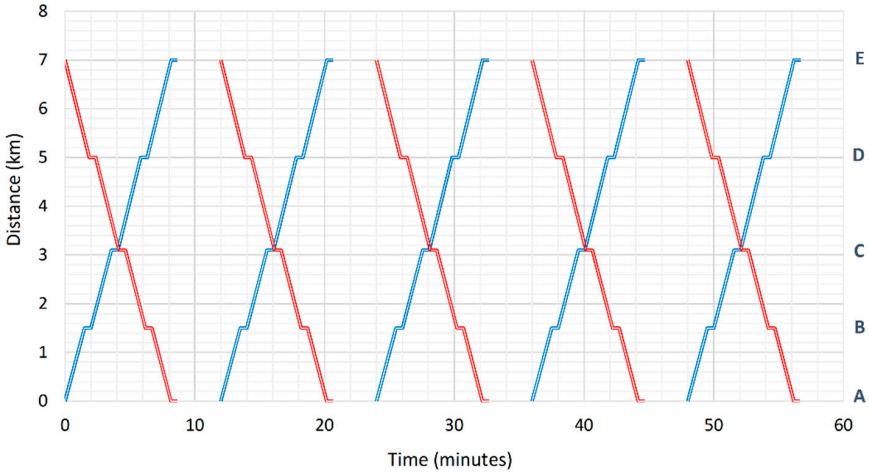

Figure A5. Simulation of 1 h tram operation between station A and B and return (12 min headway, 30 s dwell time).

Table A7 presents assumed input parameters for temperature calculations (OCS 120 mm^2 copper contact wire). The temperature input parameters were considered for Warsaw (Poland).

Table A7. Input parameters for a 120 mm^2 copper contact wire temperature calculations [44].

Parameter	Unit	Value
Initial temperature	°C	40
Ambient temperature	°C	40
Cross sectional area	mm^2	120
Diameter	mm	13.2
Maximum electrical resistance	ohms/km	0.153
Mass per unit length	kg/m	1.07
Wire specific heat (copper)	J/kg °C	385
Elevation above sea level	m	100
Air velocity	m/s	1
Stefan-Boltzman constant	W/m^2	5.67×10^{-8}
Specific mass of air	kg/m^3	1.1
The resistance temperature coefficient	–	0.004041
Solar radiation	W/m^2	1000
Solar absorptivity	–	0.95
Emission coefficient	–	0.95

References

1. European Commission. *Communication: A Clean Planet for All—A European Strategic Long-Term Vision for a Prosperous, Modern, Competitive and Climate Neutral Economy*; European Commission: Brussels, Belgium, 2018.
2. Nasri, A.; Moghadam, M.F.; Mokhtari, H. Timetable optimization for maximum usage of regenerative energy of braking in electrical railway systems. In Proceedings of the International Symposium on Power Electronics, Electrical Drives, Automation and Motion, Pisa, Italy, 14–16 June 2010; pp. 1218–1221.
3. Krol, A.; Krol, M. The Design of a Metro Network Using a Genetic Algorithm. *Appl. Sci.* **2019**, *9*, 433. [CrossRef]
4. Albrecht, T. Reducing power peaks and energy consumption in rail transit systems by simultaneous train running time control. *Power Supply Energy Manag. Catenary Probl.* **2010**, *74*, 3–12. [CrossRef]
5. Liu, H.; Zhou, M.; Guo, X.; Liu, H.; Tang, T. An abc-based subway timetable optimization model for regenerative energy utilization. In Proceedings of the IEEE International Conference on Systems, Man, and Cybernetics, Miyazaki, Japan, 7–10 October 2018; pp. 1412–1417.
6. Bocharnikov, Y.V.; Tobias, A.M.; Roberts, C. Reduction of train and net energy consumption using genetic algorithms for trajectory optimisation. In Proceedings of the IET Conference on Railway Traction Systems (RTS 2010), Birmingham, UK, 13–15 April 2010.
7. Chang, C.S.; Phoa, Y.H.; Wang, W.; Thia, B.S. Economy/regularity fuzzy-logic control of DC railway systems using event-driven approach. *IEE Proc. Electr. Power Appl.* **1996**, *143*, 9–17. [CrossRef]
8. Kim, K.M.; Kim, K.T.; Han, M.S. A Model and Approaches for Synchronized Energy Saving in Timetabling; World Congress Railway Research, Lille, France, 22–26 May 2011; 1–8. Available online: http//www.Railw.org/IMG/pdf/a4_kim_kyungmin.pdf (accessed on 10 January 2020).
9. Yang, X.; Li, X.; Gao, Z.; Wang, H.; Tang, T. A cooperative scheduling model for timetable optimization in subway systems. *IEEE Trans. Intell. Transp. Syst.* **2013**, *14*, 438–447. [CrossRef]
10. Yang, X.; Chen, A.; Li, X.; Ning, B.; Tang, T. An energy-efficient scheduling approach to improve the utilization of regenerative energy for metro systems. *Transp. Res. Part C Emerg. Technol.* **2015**, *57*, 13–29. [CrossRef]
11. Le, Z.; Li, K.; Ye, J.; Xu, X. Optimizing the train timetable for a subway system. *Proc. Inst. Mech. Eng. Part F J. Rail Rapid Transit* **2015**, *229*, 852–862. [CrossRef]
12. Douglas, H.; Roberts, C.; Hillmansen, S.; Schmid, F. An assessment of available measures to reduce traction energy use in railway networks. *Energy Convers. Manag.* **2015**, *106*, 1149–1165. [CrossRef]
13. Firpo, P.; Savio, S. Optimized train running curve for electrical energy saving in autotransformer supplied AC railway systems. *Int. Conf. Electr. Railw. A United Eur.* **1995**, 23–27. [CrossRef]

14. Ahmadi, S.; Dastfan, A.; Assil, M. Energy saving in metro systems: Simultaneous optimization of stationary energy storage systems and speed profiles. *J. Rail Transp. Plan. Manag.* **2018**, *8*, 78–90. [CrossRef]
15. Su, S.; Tang, T.; Wang, Y. Evaluation of Strategies to Reducing Traction Energy Consumption of Metro Systems Using an Optimal Train Control Simulation Model. *Energies* **2016**, *9*, 105. [CrossRef]
16. González-Gil, A.; Palacin, R.; Batty, P.; Powell, J.P. Energy-efficient urban rail systems: Strategies for an optimal management of regenerative braking energy. In Proceedings of the Transport Research Arena (TRA) 5th Conference: Transport Solutions from Research to Deployment, Paris, France, 14–17 April 2014; Volume 44, pp. 374–388.
17. Jefimowski, W.; Szeląg, A. The multi-criteria optimization method for implementation of a regenerative inverter in a 3kV DC traction system. *Electr. Power Syst. Res.* **2018**, *161*, 61–73. [CrossRef]
18. Wieczorek, M.; Lewandowski, M. A mathematical representation of an energy management strategy for hybrid energy storage system in electric vehicle and real time optimization using a genetic algorithm. *Appl. Energy* **2017**, *192*, 222–233. [CrossRef]
19. Zhang, G.; Tian, Z.; Tricoli, P.; Hillmansen, S.; Wang, Y.; Liu, Z. Inverter Operating Characteristics Optimization for DC Traction Power Supply Systems. *IEEE Trans. Veh. Technol.* **2019**, *68*, 3400–3410. [CrossRef]
20. Khodaparastan, M.; Mohamed, A.A.; Brandauer, W. Recuperation of Regenerative Braking Energy in Electric Rail Transit Systems. *IEEE Trans. Intell. Transp. Syst.* **2019**, *20*, 2831–2847. [CrossRef]
21. Meinert, M. New mobile energy storage system for rolling stock. In Proceedings of the 13th European Conference on Power Electronics and Applications, Barcelona, Spain, 8–10 September 2009.
22. Victor, H.; Aitor, M.; Haizea, G.; Ion, E.O.; Igor, V.; Haritza, C. Adaptive energy management strategy and optimal sizing applied on a battery-supercapacitor based tramway. *Appl. Energy* **2016**, *169*, 831–845. [CrossRef]
23. Radu, P.V.; Szelag, A.; Steczek, M. On-Board Energy Storage Devices with Supercapacitors for Metro Trains—Case Study Analysis of Application Effectiveness. *Energies* **2019**, *12*, 1291. [CrossRef]
24. Liu, W.; Xu, J.; Tang, J. Study on control strategy of urban rail train with on-board regenerative braking energy storage system. In Proceedings of the 43rd Annual Conference of the IEEE Industrial Electronics Society, Beijing, China, 29 October–1 November 2017; pp. 3924–3929.
25. Siemens. Increasing Energy Efficiency Optimized Traction Power Supply in Mass Transit Systems. Available online: https://www.downloads.siemens.com/download-center/download?DLA14_61 (accessed on 10 January 2020).
26. ABB Substations and Wayside Energy Storage System Support Metro in Poland. Available online: https://new.abb.com/news/detail/46010/abb-substations-and-wayside-energy-storage-system-support-metro-in-poland (accessed on 10 January 2020).
27. The Solution—EnerGstor Wayside Energy Storage. EcoActive Technologies. Available online: https://www.bombardier.com/content/dam/Websites/bombardiercom/supporting-documents/BT/Bombardier-Transportation-ECO4-EnerGstor-EN.pdf (accessed on 10 January 2020).
28. ABB, ENVILINE TM ERS energy recuperation system for DC rail transportation. Available online: https://railway-news.com/wp-content/uploads/2016/12/ENVILINE-ERS-EN.pdf (accessed on 10 January 2020).
29. Nima, G.; Javier, C.; Markus, B.; Erik, D. Review of Application of Energy Storage Devices in Railway Transportation. *Energy Procedia* **2017**, *105*, 4561–4568. [CrossRef]
30. Radu, P.V.; Drążek, Z. Analysis of wayside energy storage devices for DC heavy rail transport. *Matec Web Conf.* **2018**, *180*, 02011. [CrossRef]
31. Jefimowski, W.; Szelag, A.; Steczek, M.; Nikitenko, A. Vanadium redox flow battery parameters optimization in a transportation microgrid: A case study. *Energy* **2020**, *195*, 116943. [CrossRef]
32. Kulworawanichpong, T. Multi-train modeling and simulation integrated with traction power supply solver using simplified Newton–Raphson method. *J. Mod. Transp.* **2015**, *23*, 241–251. [CrossRef]
33. Alnuman, H.; Gladwin, D.; Foster, M. Electrical Modelling of a DC Railway System with Multiple Trains. *Energies* **2018**, *11*, 3211. [CrossRef]
34. Maxwell Datasheet 125V Heavy Transportation Module. Available online: http://www.maxwell.com/images/documents/125V_Module_datasheet.pdf (accessed on 10 January 2020).
35. Kennor, G. Overhead Line Electrification for Railways. 4th Edition. 2016. Available online: http://www.railwaysarchive.co.uk/ocs4rail/download/Overhead-Line-Electrification-for-Railways-4th-edition.pdf (accessed on 10 January 2020).

36. Saft Batteries Ion-OnBoard Regen, the Li-Ion Regenerative Hybrid Traction Battery System. Available online: https://www.saftbatteries.com (accessed on 10 January 2020).
37. He, S.; Zhang, Y.; Yang, W.; Wang, Z.; Zhao, X.; Wang, P. Investigation on the Solar Absorption Property of the Nanoporous Alumina Sheet for Solar Application. *Materials* **2019**, *12*, 2329. [CrossRef] [PubMed]
38. Girshin, S.S.; Gorjunov, V.N.; Bigun, A.Y.; Petrova, E.V.; Kuznetsov, E.A. Overhead power line heating dynamic processes calculation based on the heat transfer quadratic model. In Proceedings of the Dynamics of Systems, Mechanisms and Machines (Dynamics), Omsk, Russia, 15–17 November 2016.
39. BS IEC 60287-2-1:2015 Electric cables—Calculation of the current rating. Thermal resistance—Calculation of thermal resistance.
40. TE Transport and Environment. Recharge EU: How many charge points will Europe and its Member States need in the 2020s. In *Transport & Environment*; European Federation for Transport and Environment AISBL: Brussels, Belgium, 2020; Available online: https://www.transportenvironment.org/sites/te/files/publications/01%202020%20Draft%20TE%20Infrastructure%20Report%20Final.pdf (accessed on 31 January 2020).
41. Balcells, J.; García, J. Impact of plug-in electric vehicles on the supply grid. In Proceedings of the IEEE Vehicle Power and Propulsion Conference, Lille, France, 1–3 September 2010.
42. Dharmakeerthi, C.H.; Mithulananthan, N.; Saha, T.K. Overview of the impacts of plug-in electric vehicles on the power grid. In Proceedings of the IEEE PES Innovative Smart Grid Technologies, Perth, Australia, 13–16 November 2011.
43. Wagner, L. Chapter 27—Overview of Energy Storage Technologies. In *Future Energy (Second Edition)*; Elsevier: Amsterdam, The Netherlands, 2014; pp. 613–631. [CrossRef]
44. Eland Cables 120 mm2 Contact Wire Copper Silver. Available online: https://www.elandcables.com (accessed on 10 January 2020).